Boron Ion Implantation for Resistance Control Technique of Amorphous-InGaZnO Film

T. Ui[1], R. Fujimoto[1], K. Yasuta[1], D. Matsuo[2], T. Sakai[2], Y. Setoguchi[2], E. Takahashi[2], Y. Andoh[2] and J. Tatemichi[1]

E-mail: ui_toshimasa@nissin.co.jp
[1] NISSIN ION EQUIPMENT CO., LTD.
29, Hinokigaoka, Minakuchi-cho, Koka, Shiga, 528-0068, Japan
[2] NISSIN ELECTRIC CO., LTD.
47, Umezu-Takase-cho, Ukyo-ku, Kyoto, 615-8686, Japan
Keywords: Boron, Implantation, IGZO, Resistance

ABSTRACT

As a next-generation electronics material, amorphous indium-gallium-zinc oxide (a-IGZO) films were prepared by inductively coupled plasma sputtering on glass. In order to further utilize a-IGZO films, we carried out boron ion implantation and analyzed the implanted a-IGZO using Hall measurement and X-ray photoelectron spectroscopy. As a result, we obtain the a-IGZO sheet resistance control techniques, which can be applied to drastically sheet resistance reduction methods for a-IGZO device processing.

1 INTRODUCTION

Amorphous oxide semiconductor such as amorphous indium-gallium-zinc oxide (a-IGZO) attracts much attention for next-generation flat-panel displays due to the large band gap, light transparency, printability and low-temperature in film deposition. Using a-IGZO films, thin-film-transistors (TFTs) are realized, which show superior behavior compared with amorphous Si-based TFT [1, 2]. In order to further improve a-IGZO TFT performance via source-drain resistance reduction, plasma treatment [3], excimer laser annealing [4] and ion implantation [5, 6] methods as the sheet resistance reduction techniques were investigated. Among them, the ion implantation methods have depth control ability through insulator layers. In our previous work we elucidated that a-IGZO sheet resistance reduction can be attributed to oxygen vacancy (Vo) generated by noble gas implantation [7]. However, there is still much room for clarifying and improving the implantation method, since many injectable ion species in a-IGZO are not investigated in detail. In this work, we carried out one of the conventional ion B^+ implantation and investigation of a-IGZO thin film on glass compared with a conventional noble gas ion Ar^+ implantation cases. Electron transport properties of a-IGZO films on glass were investigated by Hall measurements. On the other hand, bonding and Vo analyses by X-ray photoelectron spectroscopy (XPS) were carried out. As a result, we obtained that a-IGZO sheet resistances and optical properties as functions of implantation energy and dose amount.

2 EXPERIMENTS and RESULTS

We prepared a-IGZO films with a film thickness 50 nm and a sheet resistance ~ 10^{13} Ω/sq. deposited by inductively coupled plasma (ICP) sputtering on a glass (0.5-mm-thick EAGLE XG), in which conditions are gas flow Ar/O_2 = 95/5 sccm, pressure 0.9 Pa, RF power 7 kW and $InGaZnO_4$ target voltage −400 V [8]. In order to decrease the sheet resistance, ion implantations of dose amount $1{\times}10^{15}$ cm^{-2} and mean projected range R_p ~ 15 nm in the a-IGZO films were carried out using ion implanter iG series [9]. Figure 1 shows a-IGZO sheet resistances without implantation (no imp.) and with B^+ or Ar^+ implantation obtained by Hall measurements. The a-IGZO sheet resistances decrease with the implantations. We find that the both implanted a-IGZO sheet resistances exhibit ~ 10^4 Ω/sq. In order to obtain sheet resistances as functions of implantation conditions, we estimated B^+ and Ar^+ implantation profiles in a-IGZO/glass structures using a simulator (Transport or Ions in Matter) [10]. Figure 2 shows typical depth profile calculation results of B and Ar concentrations in a-IGZO (50 nm)/glass structures with each ion energy E_{Ion},

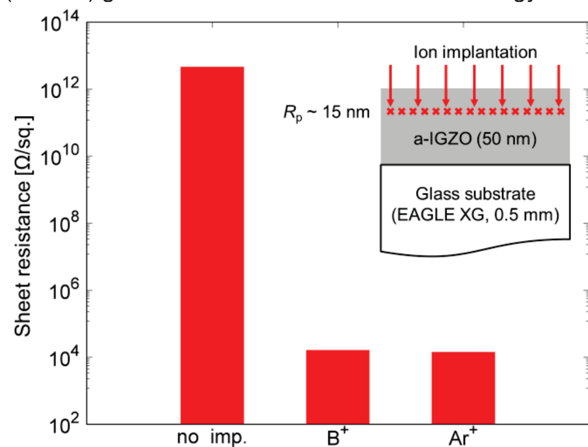

Fig. 1 50-nm-thick a-IGZO film's sheet resistances obtained by room-temperature (RT) Hall measurements without implantation (no imp.) and with each ion kind implantation, where dose amounts $1{\times}10^{15}$ cm^{-2} and mean projected range R_p ~ 15 nm. The inset shows ion implantation scheme on a-IGZO film.

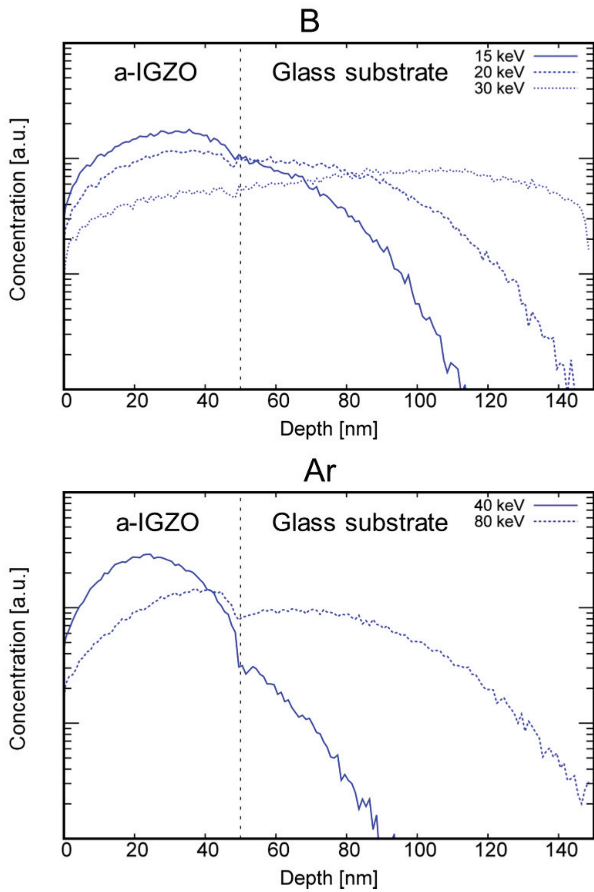

Fig. 2 B and Ar depth profiles of each ion energy E_{Ion} calculated by a simulator Transport or Ions in Matter, TRIM [10].

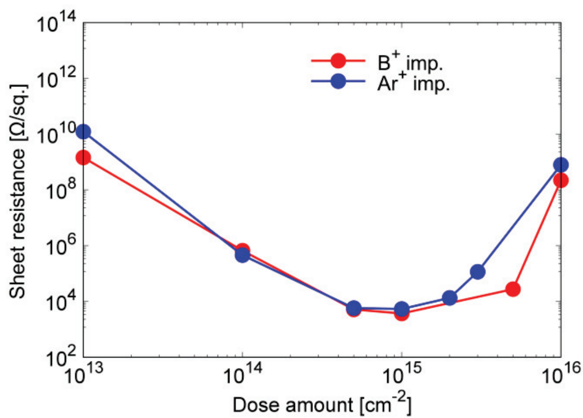

Fig. 3 a-IGZO sheet resistance as a function of B^+ and Ar^+ dose amount in the range of 10^{13} - 10^{16} cm^{-2}, where E_{Ion} are 15 keV and 80 keV respectively.

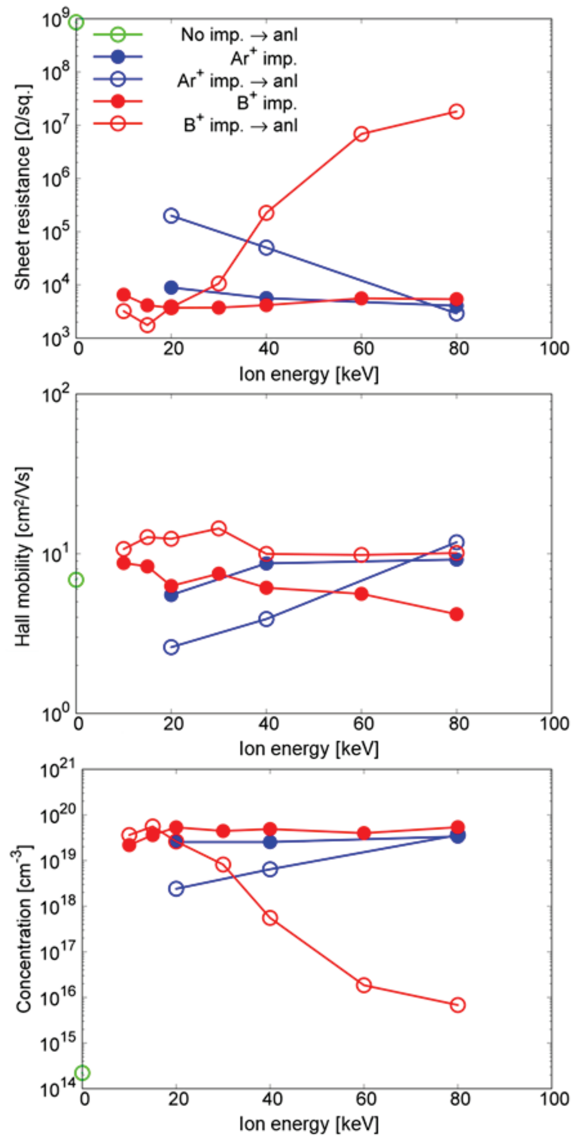

Fig. 4 Sheet resistances, Hall mobilities and concentrations as functions of E_{Ion} of 50-nm-thick a-IGZO films on glass without implantation and with B^+ implantation (B^+ imp.) or Ar^+ implantations (Ar^+ imp.) and with annealing process (anl) in N_2 ambient of 260 °C after B^+ (B^+ imp. → anl) or Ar^+ (Ar^+ imp. → anl) implantation, respectively, where dose amounts are $1{\times}10^{15}$ cm^{-2}.

where the mean projected ranges are in a-IGZO area, a-IGZO/glass interface and glass area. In order to optimize dose amounts, we carried out B^+ and Ar^+ implantations in a-IGZO/glass structures. Figure 3 shows sheet resistance as a function of B^+ and Ar^+ dose amount in the range of 10^{13} - 10^{16} cm^{-2}, where E_{Ion} are 15 keV and 80 keV, respectively. The both sheet resistances decrease with increasing in dose amount less than $1{\times}10^{15}$ cm^{-2}. On the other hand, the sheet resistance increases with increasing in dose amount

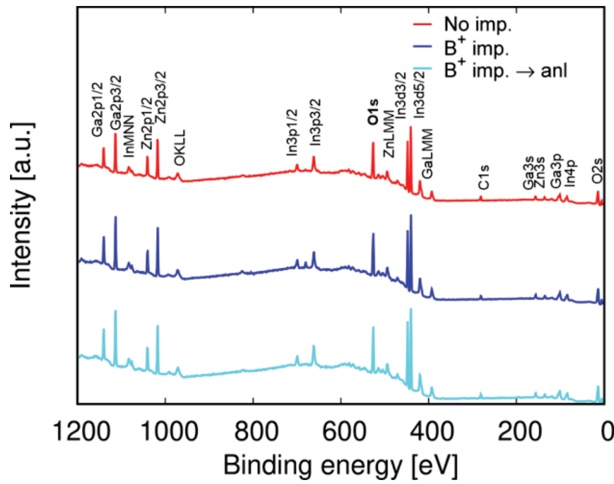

Fig. 5 X-ray photoelectron spectroscopy (XPS) global spectra for 50-nm-thick a-IGZO films without implantation and with B^+ 15 keV, 1×10^{15} cm^{-2} implantation and with annealing process after the implantation.

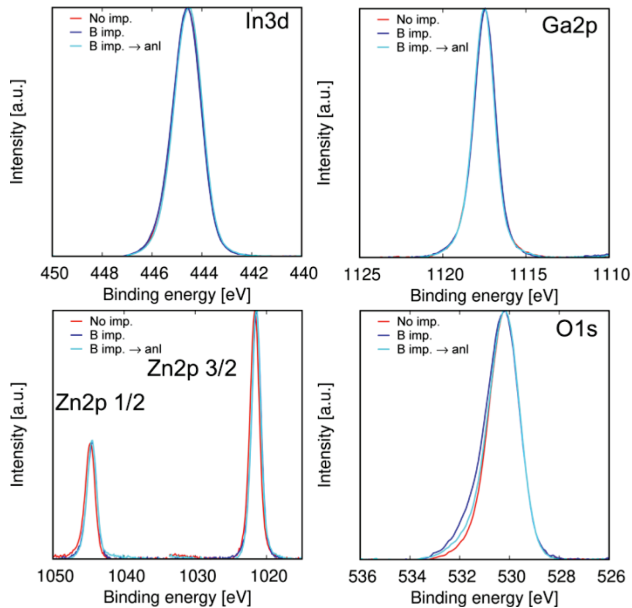

Fig. 6 XPS In3d, Ga2p, Zn2p and O1s spectra for 50-nm-thick a-IGZO films without implantation and with the B^+ implantation and with annealing process after the implantation.

larger than 1×10^{15} cm^{-2}, which indicates electron conduction path decreases due to large vacancy density. Hence, we obtained the minimum sheet resistance ~ 3×10^{3} Ω/sq. realized by optimization B^+ and Ar^+ dose amount. We carried out B^+ and Ar^+ implantations in a-IGZO/glass structures, where E_{Ion} ranges are 10 - 80 keV and 20 - 80 keV, respectively, with an uniform dose amount 1×10^{15} cm^{-2}. In addition, we prepared annealed samples in N_2 ambient of 260 °C after the implantations.

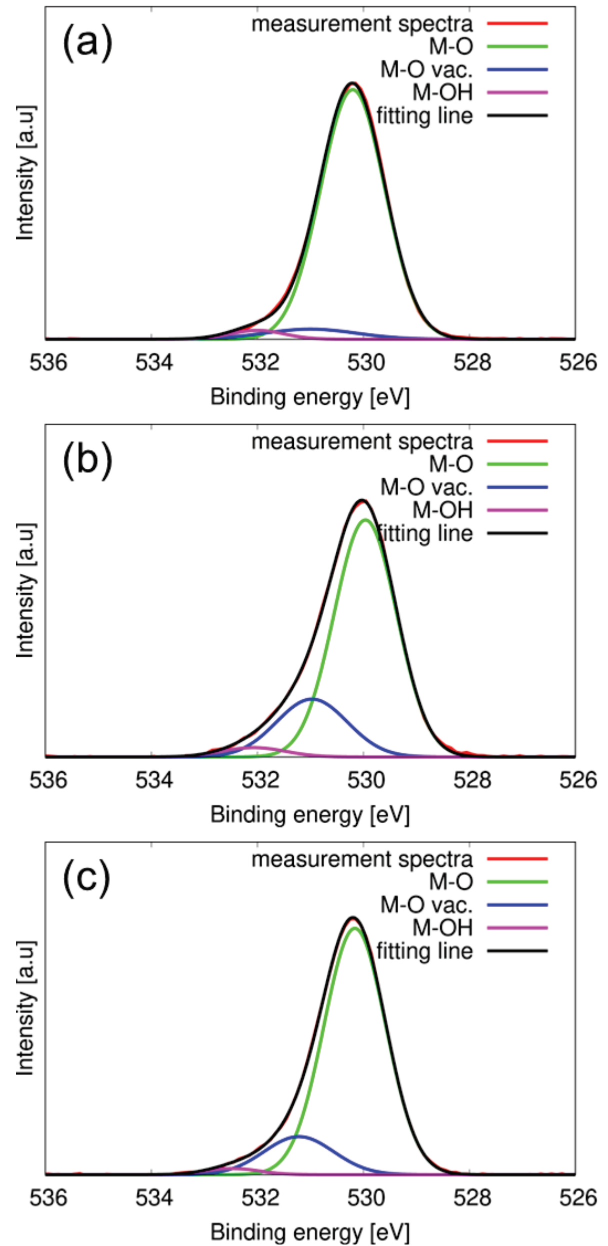

Fig. 7 XPS O1s spectra on a-IGZO films (a) without implantation and (b) with B^+ 15 keV, 1×10^{15} cm^{-2} implantation and (c) with annealing after the implantation, where the peaks of In, Zn, and Ga metal-oxygen (M-O) at 530.2 eV, M-O related to oxygen vacancy (M-O vac.) at 531.0 eV, metal-hydroxyl groups (M-OH) at 532.0 eV [11].

From Hall measurements, we obtained sheet resistances, Hall mobilities and concentrations as functions of E_{Ion} for 50-nm-thick a-IGZO films on glass with B^+ or Ar^+ implantation and without implantation as shown in Fig. 4, in which we cannot obtain concentration and Hall mobility of the a-IGZO film without implantation due to the high sheet resistance ~ 10^{13} Ω/sq. The Ar^+ implantation a-IGZO sheet resistances decrease with increasing in the E_{Ion}. In addition sheet resistance

increase amounts after the annealing decrease with increasing in the E_{Ion}, which indicates that the a-IGZO sheet resistance reduction can be attributed to electrons obtained by Vo [7] and electrons decreased by Vo repair by the annealing. Although B^+ implanted a-IGZO sheet resistance decreases with increasing E_{Ion} of 10-20 keV, a-IGZO sheet resistance decreases with increasing in the range of 20 - 80 keV, which behaviors almost corresponds to B amounts in a-IGZO films as shown in Fig. 2. In addition, we find that the increase or decrease behavior is to be emphasized after the annealing.

In order to analyze the sheet resistance reduction, XPS analyses of B^+ implantation a-IGZO were carried out. Figure 5 shows XPS global spectra for a-IGZO without implantation and with B^+ 15 keV, 1×10^{15} cm^{-2} implantation and with the annealing process after the implantation, where the binding energies were calibrated to common C1s peak at 284.6 eV. Figure 6 shows XPS In3d, Ga2p, Zn2p and O1s spectra for a-IGZO without implantation and with the implantation and with annealing process after the implantation. Although In3d, Ga2p and Zn2p peaks are almost the same shape, O1s peak shapes are deferent among each other in ~ 532 eV. Figure 7 (a), (b) and (c) show O1s spectra on a-IGZO without implantation and with the implantation and with the annealing after implantation, respectively. We can separate O1s spectra into three peaks of In, Zn and Ga metal-oxygen (M-O) at 530.2 eV, M-O related to Vo (M-O vac.) at 531.0 eV, metal-hydroxyl groups (M-OH) at 532.0 eV [11]. We find that the Vo peak increases after the B^+ implantation and the Vo peak decreases after the annealing process. In addition, the a-IGZO sheet resistance decreases even though Vo peak decreases after the annealing. Although we reported that the a-IGZO sheet resistance reduction can be attributed to the Vo in Ar^+ implantation case [7], in B^+ implantation case the XPS results indicate a possibility that not Vo but the boron itself can strongly contribute to the a-IGZO sheet resistance reduction. Hence, we obtain a-IGZO sheet resistance control techniques by optimization B^+ implantation condition.

3 SUMMARY

We investigated B^+ implantation 50-nm-thick a-IGZO films on the glass, in which a-IGZO films were prepared by ICP sputtering system. On the other hand, the B^+ implantations were carried out by using iG series. From Hall measurement, we optimize B^+ dose amount, which realize one of the minimum sheet resistance. In addition, we find that the Ar^+ implantation a-IGZO sheet resistance decreases with increasing in the E_{Ion}. On the other hand, B^+ implanted a-IGZO sheet resistances have bottom value in the range of 10-80 keV, which behaviors corresponds to B amounts in a-IGZO films, from which we obtained one of the minimum sheet resistance realized by optimization E_{Ion}. Using XPS, we obtained that the Vo relation peak increase after the B implantation and decrease after the annealing, which indicates the possibility that not Vo but the boron itself can strongly contribute to the a-IGZO sheet resistance reduction. We expect that the B^+ implantations in a-IGZO are useful as resistance control technique for a-IGZO device processing.

REFERENCES

[1] K. Nomura, H. Ohta, A. Takagi, T. Kamiya, M. Hirano and H. Hosono, ”Room-Temperature Fabrication of Transparent Flexible Thin-Film Transistors Using Amorphous Oxide Semiconductors” Nature **432** (2004) 488.

[2] T. Kamiya, K. Nomura and H. Hosono, “Origins of High Mobility and Low Operation Voltage of Amorphous Oxide TFTs: Electronic Structure, Electron Transport, Defects and Doping” J. Disp. Technol. **5** (2009) 273.

[3] H. Jeong, B. Lee, Y. Lee, J. Lee, M. Yang, I. Kang, M. Mativenga and J. Jang, “Coplanar amorphous-indium-gallium-zinc-oxide thin film transistor with He plasma treated heavily doped layer” Appl. Phys. Lett. **104** (2014) 022115.

[4] M. Nakata, H. Tsuji, Y. Fujisaki, H. Sato, Y. Nakajima, T. Takei, T. Yamamoto and T. Kurita, “Fabrication method for self-aligned bottom-gate oxide thin-film transistors by utilizing backside excimer-laser irradiation through substrate” Appl. Phys. Lett. **103** (2013) 142111.

[5] R. Chowdhurya, M. Kabirb, R. Manleyc and K. Hirschman, “Self-Aligned IGZO TFTs with Boron Implanted Source/Drain Regions” ECS Transactions **92** (2019) 135.

[6] L. Qian, W. Tang and P. Laia, “Improved Characteristics of InGaZnO Thin-Film Transistor by Using Fluorine Implant” ECS Solid State Lett. **3** (2014) 87.

[7] T. Ui, R. Fujimoto, T. Sakai, D. Matsuo, Y. Setoguchi, Y. Andoh and J. Tatemichi, “Characteristics of noble-gas-ion-implanted amorphous-InGaZnO films on glass” **27th** AM-FPD ’20 (2020) 115.

[8] D. Matsuo, R. Miyanaga, T. Ikeda, S. Kishida, Y. Setoguchi, Y. Andoh, M. N. Fujii and Y. Uraoka, “Deposition of Crystalline InGaZnO Film at Low Temperature Process by Inductively Coupled Plasma Sputtering System” the **25th** IDW ’18, FMCp7 - 2L (2018) 560.

[9] S. Dohi, H. Kai, T. Nagao, T. Matsumoto, M. Onoda, K Nakao, Y. Inouchi, J. Tatemichi and M. Nukayama, The Nissin Electric Review **62** (2017) 17.

[10] J. Ziegler and J. Biersack, Stopping Power and Range of Ion in Matter (2008).

[11] H. Kim, Y. Tak, S. Park, J. Na, Y. Kim, S. Hong, P. Kim, G. Kim, B. Kim and H. Kim, “The self-activated radical doping effects on the catalyzed surface of amorphous metal oxide films” Sci. Rep. **7** (2017) 12469.

COPYRIGHT: The copyright of this paper belongs to The Institute of Image Information and Television Engineers and The Society for Information Display.